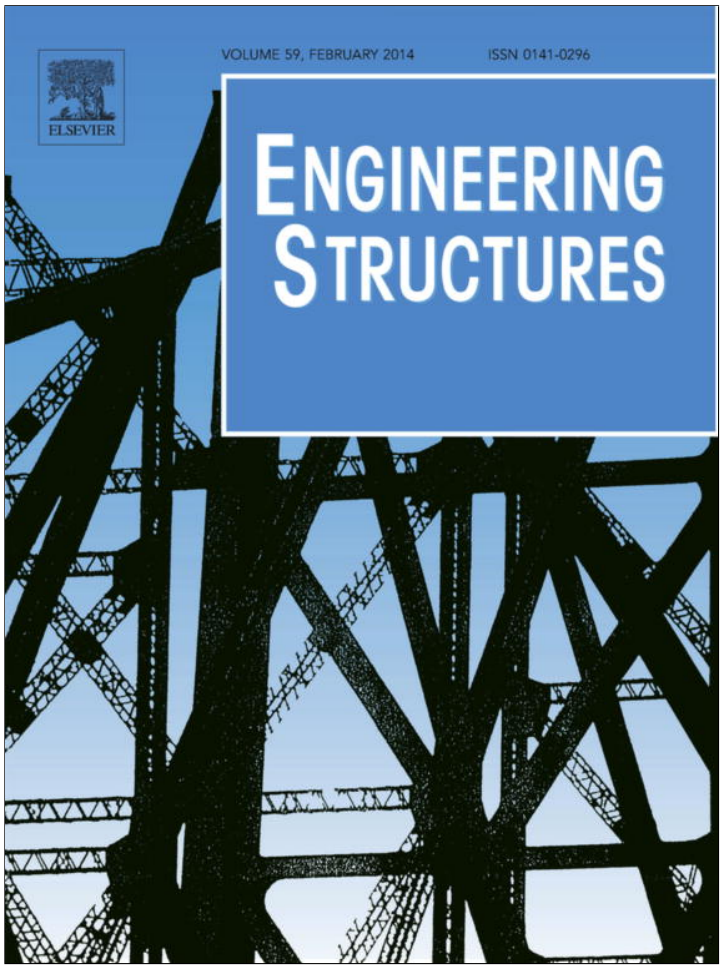

Engineering Structures 59 (2014) 536–551

Contents lists available at ScienceDirect

Engineering Structures

journal homepage: www.elsevier.com/locate/engstruct

Fully coupled, hygro-thermo-mechanical sensitivity analysis of a pre-stressed concrete pressure vessel ☆

C.T. Davie [a,*], C.J. Pearce [b], N. Bićanić [b]

[a] School of Civil Engineering and Geosciences, Newcastle University, Newcastle upon Tyne, UK
[b] School of Engineering, University of Glasgow, Glasgow, UK

ARTICLE INFO

Article history:
Received 28 August 2012
Revised 24 July 2013
Accepted 22 October 2013
Available online 15 December 2013

Keywords:
Nuclear power plant
Concrete
Hygro-thermo-mechanical
Model
Finite element analysis

ABSTRACT

Following a recent world wide resurgence in the desire to build and operate nuclear power stations as a response to rising energy demands and global plans to reduce carbon emissions, and in the light of recent events such as those at the Fukushima Dai-ichi nuclear power plant in Japan, which have raised questions of safety, this work has investigated the long term behaviour of concrete nuclear power plant structures.

A case example of a typical pre-stressed concrete pressure vessel (PCPV), generically similar to several presently in operation in the UK was considered and investigations were made with regard to the extended operation of existing plants beyond their originally planned for operational life spans, and with regard to the construction of new build plants.

Extensive analyses have been carried out using a fully coupled hygro-thermo-mechanical (HTM) model for concrete. Analyses were initially conducted to determine the current state of a typical PCPV after 33+ years of operation. Parametric and sensitivity studies were then carried out to determine the influence of certain, less well characterised concrete material properties (porosity, moisture content, permeability and thermal conductivity). Further studies investigated the effects of changes to operational conditions including planned and unplanned thermal events.

As well as demonstrating the capabilities and usefulness of the HTM model in the analysis of such problems, it has been shown that an understanding of the long-term behaviour of these safety–critical structures in response to variations in material properties and loading conditions is extremely important and that further detailed analysis should be conducted in order to provide a rational assessment for life extension.

It was shown that changes to the operating procedures led to only minor changes in the behaviour of the structure over its life time, but that unplanned thermal excursions, like those seen at the Fukushima Dai-ichi plant could have more significant effects on the concrete structures.

1. Introduction

Until recently, in many parts of the world, such as in the UK and other parts of Europe nuclear energy has fallen out of favour. But, with an ever increasing world demand for energy and the threat of global warming, nuclear power is now seen again by many as a reliable, plentiful and most importantly low carbon supply of electricity [1,2]. As a result of this, there is currently a worldwide resurgence in the development and application of nuclear power with several countries including China, India and the UK recently approving the development of new build plants [1].

However, while the international treaties to reduce carbon emissions must be enacted in relatively short timescales [3,4] the previous stagnation of the nuclear industry has resulted in a lead in time of many years before new nuclear plants can be commissioned [1]. To fill this gap, the lives of the existing stock of nuclear power plants in the UK and Europe, many of which are reaching the end of their original design lives, will need to be extended.

At the same time, the incidents following the Great East Japan earthquake in 2011, where a loss of cooling at the Fukushima **Dai-ichi plant** led to the overheating of several reactors and the release of radioactive material, have again raised questions as to the safety of nuclear power plants [5]. The main line of defence around a reactor to prevent escape of radioactive material is the containment vessel. To ensure that there is not a repeat of some of the past nuclear accidents, it is important that structural integrity of the

* Corresponding author. Address: School of Civil Engineering and Geosciences, Newcastle University, Newcastle upon Tyne NE1 7RU, United Kingdom. Tel.: +44 (0)191 222 6458.
E-mail address: colin.davie@ncl.ac.uk (C.T. Davie).

0141-0296/$ - see front matter © 2013 The Authors. Published by Elsevier Ltd. All rights reserved.
http://dx.doi.org/10.1016/j.engstruct.2013.10.033

containment vessel is maintained under all conceivable circumstances and conditions. To achieve this, it is essential that not only their mechanical properties are understood but, as they are subjected to extreme environments, also how these change over the operational life of the reactor vessel.

This paper presents an assessment of the long term behaviour of pre-stressed concrete pressure vessels (PCPV), typical of designs currently employed in the UK, that have been operating at elevated temperatures for periods in excess of 30 years. This assessment is important as it evaluates the current mechanical properties of the concrete which may then be used to ensure the structural integrity and containment of facilities whose life is to be extended.

The current state of these vessels cannot be identified without accounting for the full history of the operating conditions experienced by the structure and consideration of the effects of thermal and mechanical loads on the concrete including transport of moisture and the development of gas pressures within the pore structure of the material.

To achieve this, a fully coupled hygro-thermo-mechanical (HTM) model for concrete, originally developed during the EU FP5 Euratom *MAECENAS* (Modelling of Ageing in Concrete Nuclear Power Plant Structures) project, was employed to examine the behaviour of a typical UK PCPV over the course of its 30+ year life span under various operating conditions.

In the first instance analysis of a typical PCPV is carried out to determine the current condition of the concrete structure. A parametric analysis is then presented in which consideration is given to variations in the concrete with respect to less well characterised properties such as porosity, moisture content, permeability and thermal conductivity. Although the records from the original design and construction of UK PCPV plants are well documented and maintained, little is known about some of these properties and examination of the literature shows that very wide ranges may exist (see for example Fig. 1).

This work demonstrates that the long term behaviour of these safety–critical structures is very susceptible to small changes in material properties and a good understanding of this sensitivity is therefore vital.

Finally, a parametric study is presented in which the influence of operational conditions on the mechanical properties of the PCPV is demonstrated. This study shows how planned or unplanned events may affect the overall structural behaviour and how this may affect the safety of the PCPV. It is furthermore concluded that the numerical tool applied in this paper may be used to predict the behaviours of existing or new build concrete power plant structures (including but not limited to PCPV).[1]

2. Numerical model

This work was carried out using the fully coupled hygro-thermo-mechanical (HTM) model for concrete initially developed during the *MAECENAS* (Modelling of Ageing in Concrete Nuclear Power Plant Structures) project and presented by Davie et al. [6]. Briefly, the model treats concrete as a multiphase porous medium consisting of solid, liquid and gas phases. The solid skeleton is considered to behave isotropically and elastically under mechanical and thermal loadings, although nonlinear responses are accounted for through the consideration of transient thermal strains, transient thermal creep and an isotropic thermo-mechanical damage formulation. The 'liquid' phase considers free liquid water in pores and adsorbed water physically bound to the surface of solid skeleton. Water liberated from the solid skeleton through dehydration is considered as a part of free liquid water since chemically bound water is assumed to be initially released as liquid water. The gas phase is considered to be a mixture of dry air and water vapour, which are assumed to behave as ideal gases. Most of the material properties, both mechanical and those related to heat and mass transport, are variable, often either directly or indirectly, as a function of temperature. A complete description of the governing equations, constitutive laws and material properties may be found in [6,7,17]. A brief outline of the components of the formulation key to this work is given below and in Appendix AI.

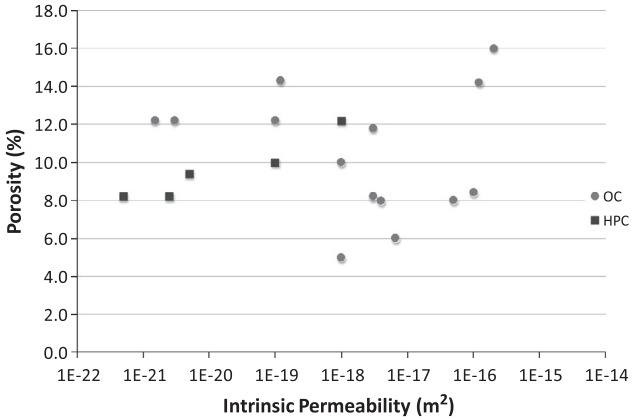

Fig. 1. Values for porosity vs. permeability for ordinary concretes (OC) and high performance concretes (HPC) described in the literature ([6–16]).

2.1. Governing equations

The model comprises four conservation equations for mass of dry air (1), mass of moisture (i.e., vapour and liquid) (2), energy (3) and linear momentum (4).

$$\frac{\partial(\varepsilon_G \tilde{\rho}_A)}{\partial t} = -\nabla \cdot \mathbf{J}_A \tag{1}$$

$$\frac{\partial(\varepsilon_G \tilde{\rho}_V)}{\partial t} + \frac{\partial(\varepsilon_L \rho_L)}{\partial t} - \frac{\partial(\varepsilon_D \rho_L)}{\partial t} = -\nabla \cdot (\mathbf{J}_V + \mathbf{J}_L) \tag{2}$$

$$(\underline{\rho C})\frac{\partial T}{\partial t} - \lambda_E \frac{\partial(\varepsilon_L \rho_L)}{\partial t} + (\lambda_D + \lambda_E)\frac{\partial(\varepsilon_D \rho_L)}{\partial t} = \nabla \cdot (k \nabla T) + \lambda_E \nabla \cdot \mathbf{J}_L \tag{3}$$

$$\nabla \cdot (\sigma' - \eta P_{Pore}\mathbf{I}) + \mathbf{b} = 0 \tag{4}$$

where ε_θ is the volume fraction of a phase $\theta(\theta = L, V, A, G, D$ refer to liquid water, water vapour, dry air, gas mixture and dehydrated water phases, respectively), ρ_θ is the density of a phase θ, $\tilde{\rho}_\theta$ the mass of a phase θ per unit volume of gaseous material, $\mathbf{J}_\theta$ the mass flux of a phase θ, $\underline{\rho C}$ the heat capacity of concrete, k the effective thermal conductivity of concrete, λ_E and λ_D are the specific heats of evaporation and dehydration, σ' is the Bishop's stress (also known as the effective stress in geomechanics), $\mathbf{I}$ the identity matrix, η is the Biot coefficient, P_{Pore} the pore pressure and $\mathbf{b}$ the body force.

2.2. Fluid transport equations

Liquid water flow in the pore structure of the concrete is assumed to be driven by pressure according to Darcy's law, and gas flow is assumed to be driven by both pressure and concentration according to Fick's law. The mass fluxes of dry air ($\mathbf{J}_A$), water

[1] While the specific example considered here is of a PCPV, the findings of the work clearly have implications for other high temperature concrete structures including but not limited to pre-stressed concrete containment vessels (PCCV). Furthermore, while the initial example considered here considers a typical existing structure, there are clear implications for assessing the long term behaviour of new build projects, under desirable and undesirable conditions.

vapour ($\mathbf{J_V}$) and liquid water ($\mathbf{J_L}$) per unit area of concrete are given by Eqs. (5)–(7).

$$\mathbf{J}_A = \varepsilon_G \tilde{\rho}_A \left(-\frac{k_g K K_G}{\mu_G} \right) \nabla P_G - \varepsilon_G \tilde{\rho}_G D_{AV} \nabla \left(\frac{\tilde{\rho}_A}{\tilde{\rho}_G} \right) \tag{5}$$

$$\mathbf{J}_V = \varepsilon_G \tilde{\rho}_V \left(-\frac{k_g K K_G}{\mu_G} \right) \nabla P_G - \varepsilon_G \tilde{\rho}_G D_{AV} \nabla \left(\frac{\tilde{\rho}_V}{\tilde{\rho}_G} \right) \tag{6}$$

$$\mathbf{J}_L = \varepsilon_L \rho_L \left(-\frac{K K_L}{\mu_L} \right) \nabla P_L \tag{7}$$

where K is the intrinsic permeability of the dry concrete, K_θ, μ_θ and P_θ are the relative permeability, dynamic viscosity and pressure of the phase θ, k_g is the gas-slip modification factor and D_{AV} is the coefficient of diffusion for the dry air/water vapour mixture within the porous concrete.

The moisture content and saturation of the concrete is controlled by the relative humidity in the pore space via the sorption isotherms (8).

$$\varepsilon_L = \frac{\varepsilon_{Cem} \rho_{Cem}}{\rho_L} \cdot f\left(\frac{P_V}{P_{Sat}}, T \right) \tag{8}$$

where $\varepsilon_{Cem}\rho_{Cem}$ is the cement content per unit volume of concrete, P_V is the vapour pressure, P_{Sat} is the saturation vapour pressure and (P_V / P_{Sat}) is the relative humidity (see AI.3).

The porosity, ϕ, of the concrete then controls the size of the gas volume fraction, ε_G (9).

$$\phi = \varepsilon_L + \varepsilon_G \tag{9}$$

2.3. Mechanical constitutive equations

The total strain ($\boldsymbol{\varepsilon}$) of the solid skeleton is considered to consist of elastic strain ($\boldsymbol{\varepsilon}^e$), free thermal strain ($\boldsymbol{\varepsilon}^{ft}$) and load induced thermal strain ($\boldsymbol{\varepsilon}^{lits}$), i.e.,

$$\boldsymbol{\varepsilon} = \boldsymbol{\varepsilon}^e + \boldsymbol{\varepsilon}^{ft} + \boldsymbol{\varepsilon}^{lits} \tag{10}$$

The effect of mechanical and thermal loading on the elastic stiffness is accounted for by an isotropic scalar damage model where the classical damage formulation, with a single mechanical damage parameter, ω, has been modified to include a second thermal damage parameter, χ.

$$\boldsymbol{\sigma}' = (1-\omega)(1-\chi)\mathbf{D}_0 : \boldsymbol{\varepsilon}^e \tag{11}$$

where σ' is the Bishop's stress, $\mathbf{D_0}$ is the initial elasticity tensor, ω is the mechanical damage parameter, accounting for the loss of the elastic stiffness caused by the micro-fracturing of concrete that develops under loading and χ the thermal damage parameter, accounting for the reduction of the elastic stiffness due to thermally induced degradation of the cement paste.

The free thermal strain rate is calculated by way of Eq. (12):

$$\dot{\varepsilon}^{ft}_{ij} = \alpha \dot{T} \delta_{ij} \tag{12}$$

where α is a non-linear, temperature dependent coefficient of thermal expansion, $\dot{T}$ is the rate of temperature change and δ_{ij} is the Kronecker delta.

The load induced thermal strain rate is calculated as shown in Eq. (13):

$$\dot{\varepsilon}^{lits}_{ij} = \frac{\beta}{f^0_c} \left((1-v_c)\sigma'^{-}_{ij} - v_c \sigma'^{-}_{kk} \delta_{ij} \right) \dot{T} \quad \text{for } \dot{T} > 0 \tag{13}$$

where β is the coefficient of load induced thermal strain (AI.5), f^0_c is the initial compressive strength, v_c is the lateral component of the load induced thermal strain (similar to Poisson's effect) and σ'^{-}_{ij} is the negative (compressive) projection of the Bishop's stress tensor, σ'_{ij}.

2.4. Numerical solution

Using the standard Finite Element approximation, the chosen primary variables of displacements, u, temperature, T, gas pressure, P_G, and vapour content, $\tilde{\rho}_V$, are expressed in terms of their nodal quantities:

$$\mathbf{u} = \mathbf{N}_u \mathbf{a}; \quad T = \mathbf{N}_T \mathbf{T}; \quad P_G = \mathbf{N}_P \mathbf{P}_G; \quad \tilde{\rho}_V = \mathbf{N}_\rho \boldsymbol{\rho}_V \tag{14}$$

where $\mathbf{N}_\theta$ are the shape functions, $\mathbf{a}$, $\mathbf{T}$, $\mathbf{P}_G$ and ρ_V are the nodal variables, and the resulting system of discrete equations is expressed in matrix form as:

$$\mathbf{C}\dot{\mathbf{x}} + \mathbf{K}\mathbf{x} = \mathbf{f}^{ext} \tag{15}$$

The discrete set of Eq. (15) is also discretised in time using a finite difference scheme as:

$$\mathbf{x}^{t+\alpha\Delta t} = (1-\alpha)\mathbf{x}^t + \alpha \mathbf{x}^{t+\Delta t} \quad \dot{\mathbf{x}}^{t+\alpha\Delta t} = \frac{\mathbf{x}^{t+\alpha\Delta t} - \mathbf{x}^t}{\Delta t} \tag{16}$$

where Δt is the time increment, $\mathbf{x}^t$ and $\mathbf{x}^{t+\Delta t}$ denote the unknowns at times t and $t + \Delta t$ respectively and α is a constant ($0 \leqslant \alpha \leqslant 1$).

Boundary conditions are defined for the primary variables as either Cauchy type (mixed) boundary conditions, where energy and mass transport takes place across the boundary dependent on the conditions internal and external to the concrete, or Dirichlet type (fixed) boundary conditions, depending on the nature of the physical boundaries themselves.

2.5. Model validation

This model has been validated through extensive application to numerous problems ranging from isothermal drying to rapid fire loading, and has been demonstrated capable of accurately representing the multi-phase, macro-scopic behaviour of concrete exposed to elevated temperatures, e.g. [6,7,17].

3. Numerical analyses

The results from a total of 32 analyses are presented covering a range of parametric investigations, as described in the following sections. The scale and complexity of the PCPV structure, which is typical of those still in use in several plants in the UK, is illustrated by the schematic shown in Fig. 2 and finite element meshes shown in Fig. 3. The analyses conducted for this work are of two types. The first type employs the axi-symmetric representation of the PCPV (Fig. 3b) to conduct full HTM analyses of the vessel. The second type employs the simplified axi-symmetric representation of a slice through the outer wall of the vessel (Fig. 3c) in order to conduct a parametric sensitivity study of the properties affecting heat and mass transport in the concrete.

In all cases the boundary conditions for the analyses are set up such that the outside of the pressure vessel is considered to be open to the atmosphere and can thus freely exchange vapour and heat (see Fig. 3). Typical values of atmospheric properties are maintained with a constant pressure of 0.1 MPa and temperature of 15 °C. For all but one analysis, the relative humidity of the atmosphere is set to 70%.

The inside of the pressure vessel is considered to be sealed to gas flow, as representative of the internal steel liner, and has applied a set of prescribed temperatures, which vary in time according to the operational condition of the reactor, as exemplified in Fig. 4c. For the full HTM analyses the typical magnitude of the temperatures vary depending on location around the inside surface,

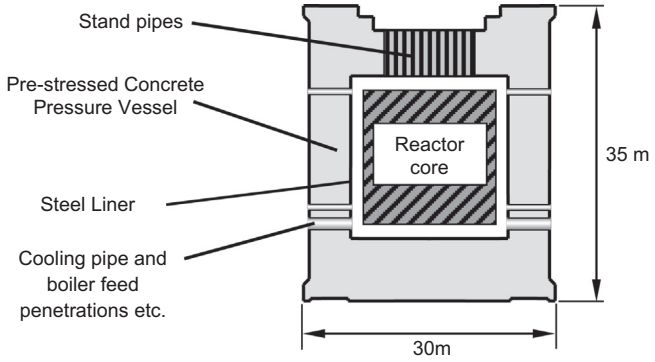

Fig. 2. Schematic illustration of typical PCPV.

from a minimum operating temperature of 37 °C to a maximum of 85 °C. For the simplified 'slice' analyses a single temperature profile is considered.

For the full axi-symmetric analysis three types of mechanical boundary condition were also required. Firstly, the base of the typical structure rests on a stiff but deformable neoprene layer represented by elastic spring boundaries along the inner part of the lower edge of the mesh. Secondly, to represent the pre-stressing loads provided by helical tendons tensioned throughout the outside wall of the structure equivalent vertical and horizontal nodal loads were applied to the top and bottom boundaries as well as internal elements. The third set of mechanical boundary conditions were nodal forces applied to the internal surface of the vessel to represent the internal pressures acting on the structure during operation.

Typical variations of the pre-stressing forces over time, accounting for creep in the tendons, and of the internal pressures, dependent on the operational conditions of the reactor over its life time, are shown in Fig. 4.

The details of the typical boundary condition data was provided by the operators during the *MAECENAS* project from records of construction and operation [18]. Specific details of the applied boundaries are discussed as necessary in the following sections.

4. Numerical investigations

4.1. HTM analysis of PCPV

This first analysis was conducted in order to determine the current state of a typical PCPV structure resulting from its 30+ year operating life time. As described in the previous section a full HTM analysis was carried out using the axi-symmetric mesh shown in Fig. 3b and applying representative temperature, pressure and load histories as recorded over the life time of the structure (Fig. 4).

As can be seen from Fig. 4 the first approximately 7 years of the structures life were considered the construction phase during which the reactor was not commissioned and no increased temperatures were experienced by the structure. However, during the construction phase, after approximately 4½ years and following tensioning of the pre-stressing tendons, a proof pressure test was conducted during which the internal pressure was raised to nearly 5 MPa, well in excess of the typical operating pressures of 3.9 MPa. Following the construction phase and reactor start up, it may be seen that the temperatures and pressures on the internal faces of the vessel increased smoothly to their operational values and then remained constant for the life time of the structure, with the exception of two planned outages after approximately 9 years and 22 years of operation.

For this analysis a best estimation of the initial material properties was employed, taking what data was available from the operator's construction and maintenance records for the typical structure. The initial material properties employed are listed in Table 1 [18].

The results of the analysis can be seen in Figs. 5–7. Fig. 5a shows the temperature profile in the concrete structure. This profile, taken at the end of the modelled life time is typical of the near steady state conditions found to develop during long term operation. It can be seen that the temperature on the inside surface varies with location, the hottest parts being at the top of the vessel. It can also be seen that the temperature field extends most of the way through the ~5 m thick concrete structure and so, although at relatively low levels, much of the concrete is subject to effects including thermal expansion, transient thermal creep and thermal damage (i.e. degradation of the concrete properties and the development of micro-cracking as a result of heating).

Fig. 5b shows the gas pressure field in the concrete structure where pressures have developed inside the pore space of the porous concrete material as a result of the evaporation of liquid water and the subsequent development of water vapour. As can be seen and expected, this field corresponds with that of the temperatures, with the highest pressures developed in the hottest areas of the concrete, nearest the inner steel liner and in the upper parts of the vessel. While the maximum pressures predicted here are of the order of 0.29 MPa and pose few implications for the structure, it is notable that under relative mild conditions pressures of nearly

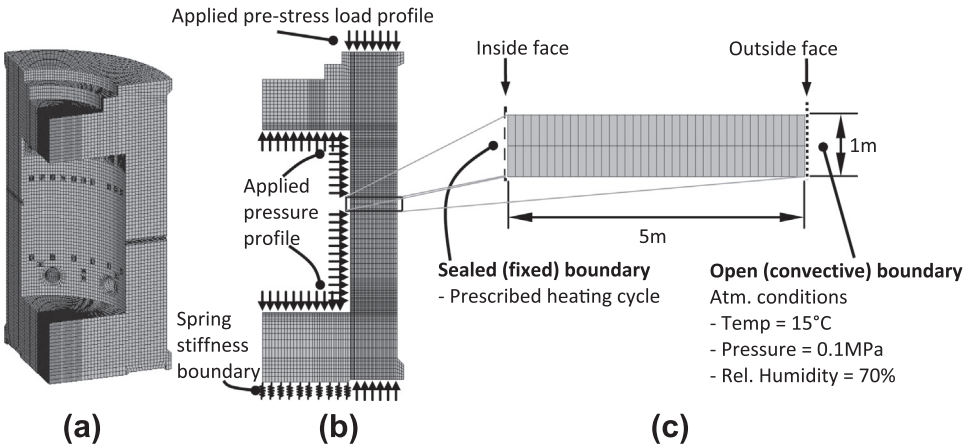

Fig. 3. (a) Quarter symmetry 3-dimensional finite element mesh of typical PCPV, (b) simplified axi-symmetric finite element mesh of typical PCPV, (c) axi-symmetric finite element mesh of slice through outer wall of typical PCPV.

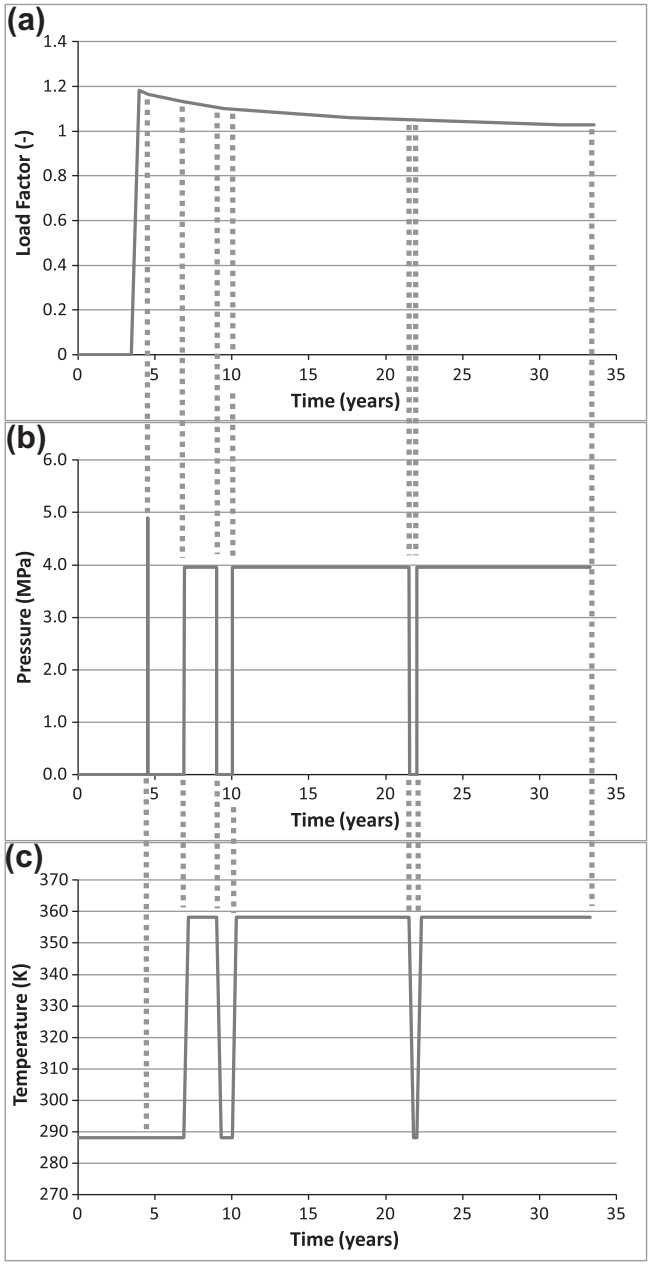

Fig. 4. (a) Load factor applied to pre-stressing tendon loads over life time of PCPV, (b) Internal pressures applied to internal surface of PCPV during operation over its life time, (c) Typical temperature profile applied to internal surface of PCPV during operation over its life time.

3 times atmospheric pressure developed close to the steel liner that provides containment and that most of the structure is subject to elevated pressures. The development of these pressures and potential implications will be considered further in the following analyses.

Corresponding with the gas pressure field, the saturation of the pressure vessel with liquid water may be seen in Fig. 5c. It may be noted that a significant proportion of the vessel is subject to drying from the initial ~75% saturation to a minimum of ~40% at the hottest parts. Nonetheless, all of the concrete remains wet to some extent and in fact some of the deeper part of the vessel experience a slight increase in saturation (to a maximum of ~77%) as moisture moves from the hotter parts of the vessel and re-condenses in the cooler parts. It may also be seen that the outer most parts of the concrete experience a slight drop in saturation as drying to the atmosphere takes place over time.

The mechanical response of the structure over the modelled life time is illustrated in Fig. 5d–g. The deformation of the structure may be noted in Fig. 5d–f and, although exaggerated in these figures, it can be seen that the shape of the structure changes considerably during the cold and hot operational phases. During the cold phases, pre-operation (Fig. 5d) and at the end of the second outage (Fig. 5e) it may be seen that the wall of the structure bends inwards under the confining loads of the pre-stressing tendons. However, during the hot phases, the wall of the structure bends outwards, under the combined actions of restrained thermal expansion and internally applied pressures.

Relatively, the deflections are not large, reaching a maximum lateral displacement at the end of the modelled life time of approximately 1.3 mm, at mid-height on the outside of the wall of the structure. However, in considering the size and stiffness of the structure this may be considered noteworthy.

It may be further noted that the lateral deformation increases over the life time of the structure. This is illustrated by Fig. 5e, where it can be seen that, although the structure has returned to an inwardly bending configuration during the (cold) outage, the pattern of deformations is different to that seen at the end of the construction phase (Fig. 5d). This is further illustrated by Fig. 6, which shows the lateral deformation in time at mid-height on the outside of the wall of the structure.

As can be seen, a large inward (negative) deformation occurs initially when the confining pre-stress loads are applied during the construction phase. An outward (positive) spike occurs due to the proof pressure test after approximately 5 years and this is then followed by a series of large outwards and inwards displacements that are associated with the bending behaviour of the structure during initial heat up of the reactor and the two planned outages. However, overlying all of these, a gradual outwards increase in deformation with time may be seen. This is due firstly to the creep of the pre-stressing tendons which gradually relax

Table 1
Initial concrete properties and boundary conditions.

Property	Value	Boundary condition		Value
Tensile strength	4 MPa	Internal Boundary	Temp.	Prescribed
Compressive strength	60 MPa		Pressure	Undefined (sealed conditions)
Porosity	0.10		Vapour	Undefined (sealed conditions)
Permeability	2.0×10^{-18} m^2		Mechanical	Applied loads according to pressure profile (Figs. 3b and 4b)
Mass moisture content/ saturation	3.3%/~75%	External Boundary	Temp.	15 °C
Thermal conductivity	Average Eurocode curve [19] (AI.2)		Pressure	0.1 MPa
Density	2270 kg/m^3		Vapour	0.00898 kg/m^3 ≡ 70% Relative Humidity
			Mechanical	Applied loads according to pre-stressing load profile (Figs. 3b and 4a) Spring boundaries along base (Fig. 3b)

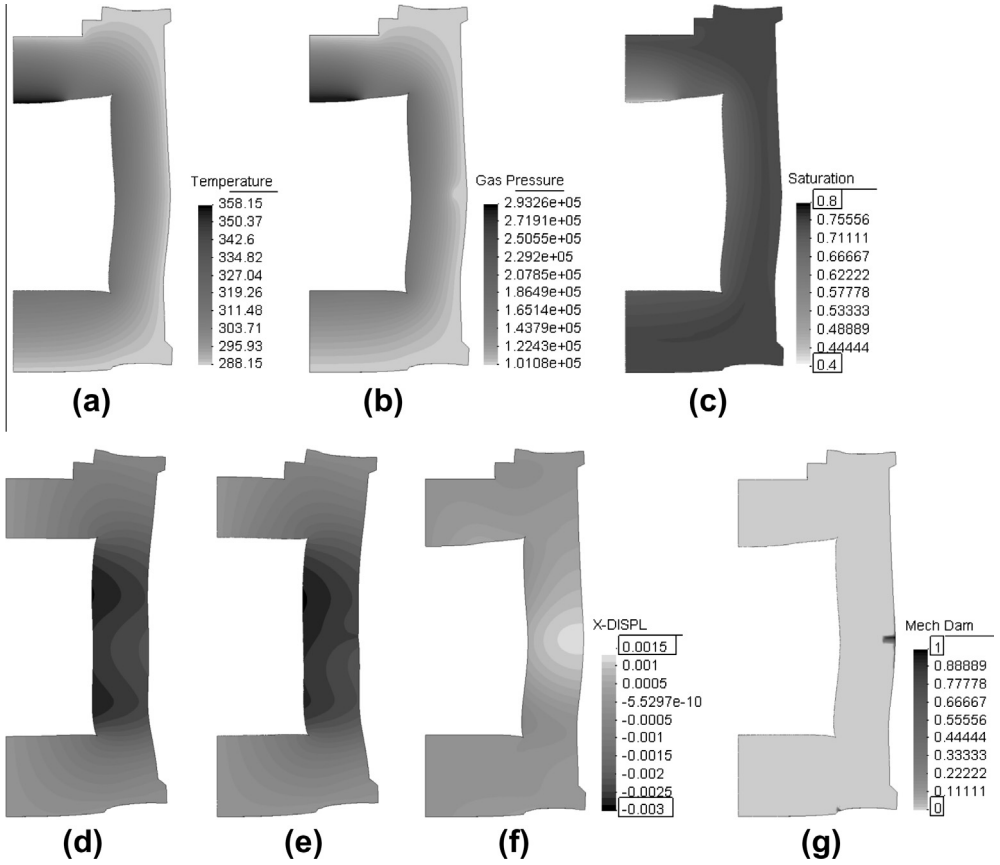

Fig. 5. Deformation of structure at an exaggerated scale (×500) showing (a) temperature [K] field under long term operational conditions, (b) pore gas pressure [Pa] field under long term operational conditions, (c) liquid water saturation field under long term operational conditions, (d) lateral displacements [m] under cold conditions, pre initial heat up phase, (e) lateral displacements [m] at end of second outage, (f) lateral displacements [m] under long term operational conditions, (g) mechanical damage field under long term operational conditions.

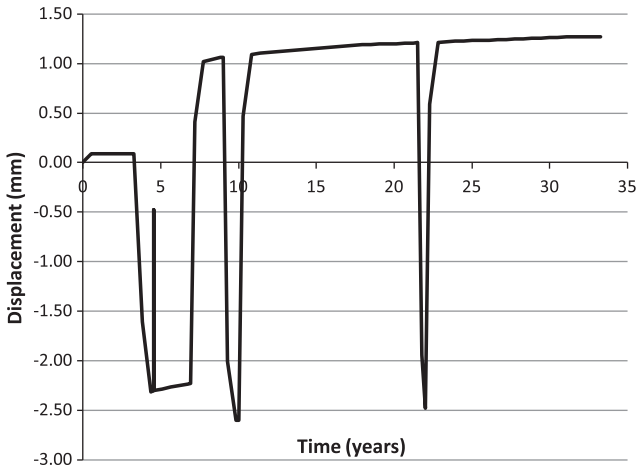

Fig. 6. Lateral displacements at mid-height on the outside of the wall of the structure.

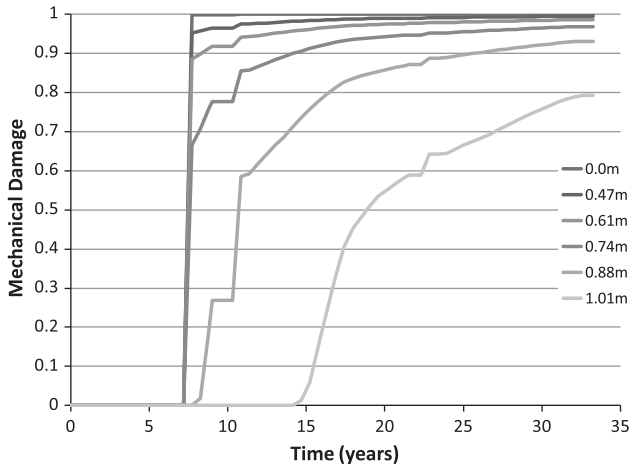

Fig. 7. Mechanical damage development (see Fig. 5g) at points measured from the outside surface of the structure, in time.

the confining loads (Fig. 5a), and secondly, to the development of mechanical damage, which can be seen in Fig. 5g.

The damage occurs when the wall of the structure bends outwards during the hot operational phases, resulting in the development of tensile stresses, and forms in a zone along the outside face of the structure and deeper into the structure at mid-height. While this damage may not represent an observable phenomenon in terms of visual inspection of the pressure vessel, it does indicate that the material in this area, and therefore the structure, has degraded from its original strength, stiffness and structural integrity; the reduction in stiffness leading to the increase in deformation.

Upon further examination it may be noted that the level of damage itself increases over the life time of the structure. Fig. 7 shows the development of damage in time at 6 points along the length of the damage zone seen in Fig. 5g.

As can be seen damage originally develops at the outside of the structure (0.0 m) upon first heat-up (see Fig. 4c) as a result of normal operating conditions. Damage then begins and continues to develop at other points deeper in the structure, sometimes, but not always, concurrent with restart of the reactor after the two planned outages. This progressive development further explains the increase in lateral deformations noted earlier, which develop as a result of the progressive decrease in structural stiffness.

Overall, it is likely that the growth in damage is due to the gradual decrease in the confining loads resulting from the creep in the pre-stressing tendons combined with the effects of transient thermal creep (which, due to its monotonic occurrence, can lead to the development and 'locking in' of tensile stresses during cool down [20]). The deepest point at which damage develops is approximately 1 m from the outside surface of the vessel. This is reasonably significant in terms of the overall size of the structure but the damage is likely to be micro-structural rather and observable macro-scale fractures and furthermore, the deflections remain very small. So the results do not suggest an imminent loss of structural integrity or a particular safety concern. However, they do suggest that detailed analysis is required over the life time of the structure in order to provide a rational assessment for life extension. It can also be seen that in terms of new build, this type of analysis may be employed very usefully to inform design decisions such as the type and magnitude of pre-stress loads.

4.2. Simplified slice analysis – parametric study

As described previously, following the full analysis described in Section 4.1, a set of 22 analyses were carried out in order, firstly, to conduct a parametric investigation of the effects of various, less well identified material properties; porosity, moisture content, permeability, and thermal conductivity, and secondly, to conduct a sensitivity study in relation to operating conditions experienced by the structure; timing and length of shut downs, environmental conditions and extended operating life. These investigations focused on the transient heat and mass transport in the structure and so a simplified slice model was employed, as shown in Fig. 3c. Mechanical behaviour was not specifically considered. As before, unless specified as part of the analysis, the typical recorded temperature history was applied to the inner face of the structure over the full 30+ year operating life time, and again, unless specific to the analysis all initial material properties remained the same as those applied in the first analysis (Table 1). Of principal concern during these analyses were the temperature profiles across the structure and the gas pressures built up in the pore space of the concrete at the internal boundary. The temperature affects material properties such as strength and stiffness, which degrade with increasing temperatures, transient strains (both thermal expansion and transient thermal creep), and the development of damage. The gas pressures effectively apply a tensile stress internally to the concrete and therefore have implications for the development of damage. At the internal boundary of the concrete structure it is also possible that these pressures will act directly on the steel liner.

4.2.1. Porosity

Porosity is the space available in the pore structure of the concrete in which fluids (liquid and gas) can be present and through which they can flow. It therefore controls fluid pressures and flow behaviour and so may have a significant bearing on the overall couple HTM behaviour of a structure such as a PCPV.

Unfortunately porosity it is not usually specified in design or even measured for in existing structures, so its value is not generally known. Examination of the literature finds numerous values for the porosity of concrete quoted ranging from around 5% to around 16%. These include values for high performance and ordinary concrete with a wider range being seen for the latter (see Fig. 1).

However, little pattern or trend is discernible in the quoted values and it is difficult to directly relate the porosities to any other factor or property of the concretes. Without laboratory measurements it is therefore very difficult to identify the value for a given concrete.

Although the value of 10% employed in the first analysis was a best estimate from the information available, it is far from certain that this is exactly correct. Therefore, to determine the significance of the porosity for the behaviour of the PCPV three separate analyses were conducted with porosities of 5%, 10% and 16%.

Fig. 8a shows the near steady state temperature profile developed across the width of the PCPV wall during periods of normal operating conditions. As can be seen, although it may be expected that variations in the moisture content and transport through the wall, as may be caused by variations in porosity, could affect the heat transfer behaviour (and vice versa) through coupling of properties such as the specific heat capacity, virtually no effect was seen in this case. So it may be stated that the porosity has no significant effect on the heat transfer and this was in fact found to be the case for all properties investigated here.

In relation to the moisture transport, however, there are two points of note. Firstly, it may be seen that the gas pressures at the inner boundary of the structure continued to develop and change over the life time of the structure (Fig. 8b). Clear changes in the gas pressure can be seen that are easily identifiable with the relatively rapid changes in temperature associated with first heat up and the two planned outages. However, the size of the structure and the relatively low operating temperatures mean that the drying process is extremely slow and is not complete even after 30+ years of operation (Fig. 8c). Relatively, the lower porosity materials dry faster, where an initial saturation of 75% represents a smaller total volume of water, and it might be expected that the drying rate would therefore be proportional to the porosity. However, the drying rate is also affected by capillary suction, which acts to hold the water in place. This is lost below a saturation of 0.55, which is representative of the point of maximum curvature of the capillary menisci and the point at which they can no longer be supported. As can be seen in Fig. 8c, when capillary suction is lost, the drying rate then increases.

The second point of note is that the porosity of the concrete has a reasonably significant effect on gas pressure build up. With the original porosity of 10% the gas pressure peaked after each heat up phase and reached an overall peak after approximately 25 years, after which it slowly decreased. The maximum pressure reached was just under 0.3 MPa. With the lower porosity of 5%, where there is less space and therefore less water available for evaporation, the gas pressure decreased slowly over the whole life time of the structure and reached a maximum pressure of less than 0.2 MPa. However, with the higher porosity of 16%, where most water is available for evaporation, it can be seen that the gas pressure continued to rise over the full life time of the structure. The maximum pressure reached after approximately 33 years approached 0.6 MPa. It should be noted that while there may be a tangible link between porosity and permeability, here permeability remained constant and variations in permeability for constant values of porosity are considered later.

So, for the feasible range of porosities found in the literature it may be seen that the gas pressure ranges up to 6 times atmospheric pressure. While the magnitudes in question are not in themselves necessarily significant at this point in terms of the loads applied to the concrete or steel liner, it may been seen that for higher porosities the conditions worsen over the life time of the structure and the observed variation is significant enough so as to suggest that a reasonable understanding of the concrete

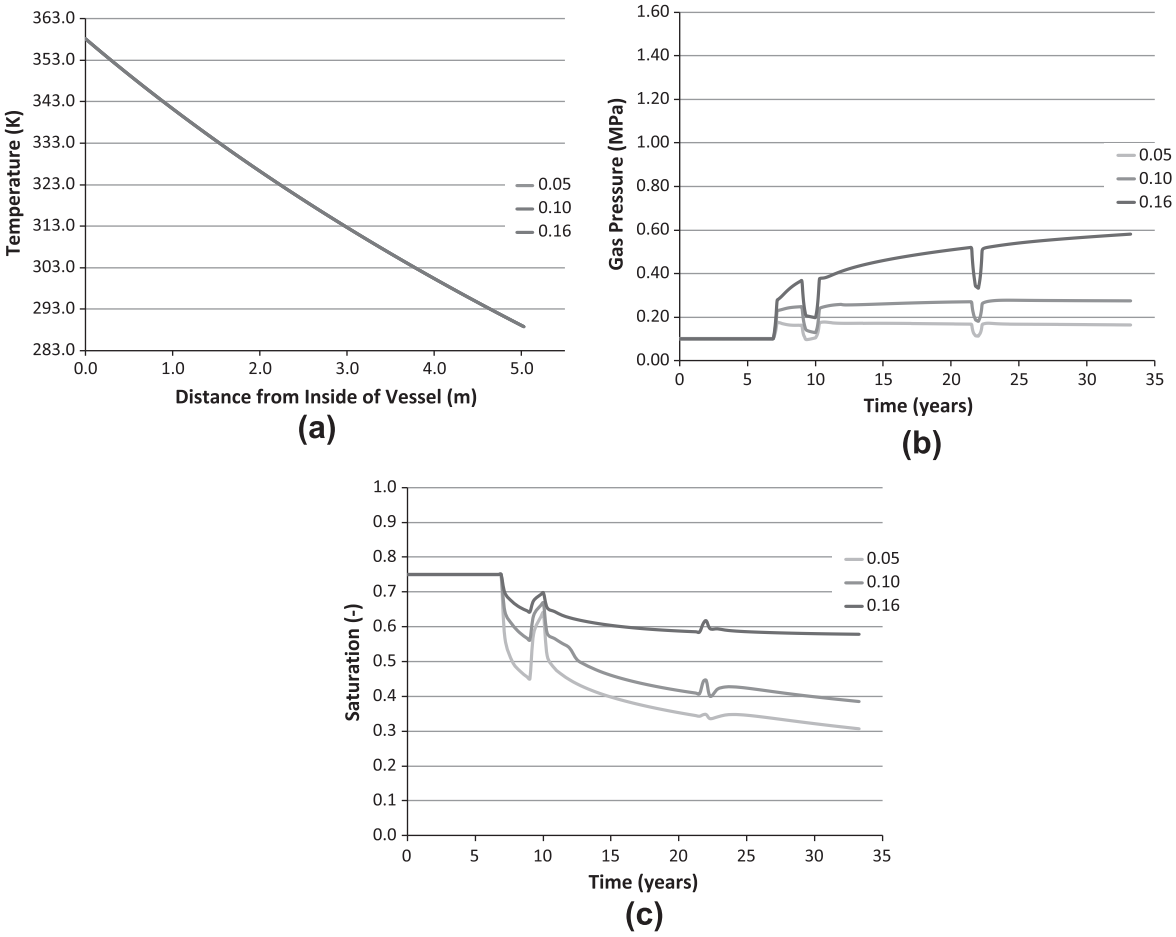

Fig. 8. Results of analyses with various porosities showing (a) steady state temperature profiles across the width of the structure, (b) gas pressures at the inner boundary in time and (c) the liquid water saturation at the inner boundary in time.

porosity is required in order to gain a reasonable prediction of the moisture transport in the concrete.

4.2.2. Moisture contents

As mentioned in relation to the porosity, the gas pressures that can develop in the concrete are directly related to the amount of water available for evaporation. They are therefore fundamentally related to the initial moisture content of the concrete, which is a function of the concrete mix and of the atmospheric conditions during curing, with which the water in the porous concrete will equilibrate. Furthermore, the amount of water present in the concrete will affect both the thermal conductivity and the heat capacity of the concrete and will therefore affect the heat transfer. Since, as discussed previously, the development of gas pressures in the pore space of the concrete could lead to the development of damage, it may be important to consider the precise moisture content of the concrete.

Again, however, the true moisture content is not easily established due to its dependence on the original design mix and the environmental conditions subsequent to construction, and so to determine its significance a range of moistures have been investigated. Three analyses were run using the simplified slice model with initial saturations of 65%, 75% and 85% (approximately equivalent to mass moisture contents of 2.9%, 3.3% and 3.8%).

From Fig. 9a it can be seen that the gas pressures were also influenced by the initial moisture content although the range and effect was much less than that caused by the variation in porosity, with a maximum pressure of about 0.35 MPa predicted. Moisture content may therefore be considered to be of low significance when considering the structural performance of the PCPV.

Notwithstanding this conclusion, it may be seen that while for mass moisture contents of 3.3% and below the gas pressures peaked before reducing slowly over the life time of the structure, for a mass moisture content of 3.8% the gas pressures continued to rise over the whole life time of the structure and therefore represented a worsening condition.

The initial moisture content also affected the drying response of the structure (Fig. 9b). Again, the drying rates increased for the lower initial moisture contents as the saturation dropped below 0.55 and in these cases the drying process was not complete even after 30+ years of operation. In contrast, with the highest initial moisture content the saturation remained above this critical point and levelled off at a steady state, implying equilibrium with the atmosphere, only a few years after each outage. This higher 'final' moisture content could have significance for structural performance in the light of operational conditions or temperature excursions experienced in later life (see Sections 4.3 and 4.4).

4.2.3. Permeability

While laboratory testing is desirable to determine the porosity and moisture content of a concrete, estimates for these properties may be made if the original mix design is known and assumptions are made about the degree of hydration. However, no such estimate may be made as to the permeability of the concrete as, while this can be linked to the porosity, it is controlled by the microstructure of the concrete and this is not easily related to mix design.

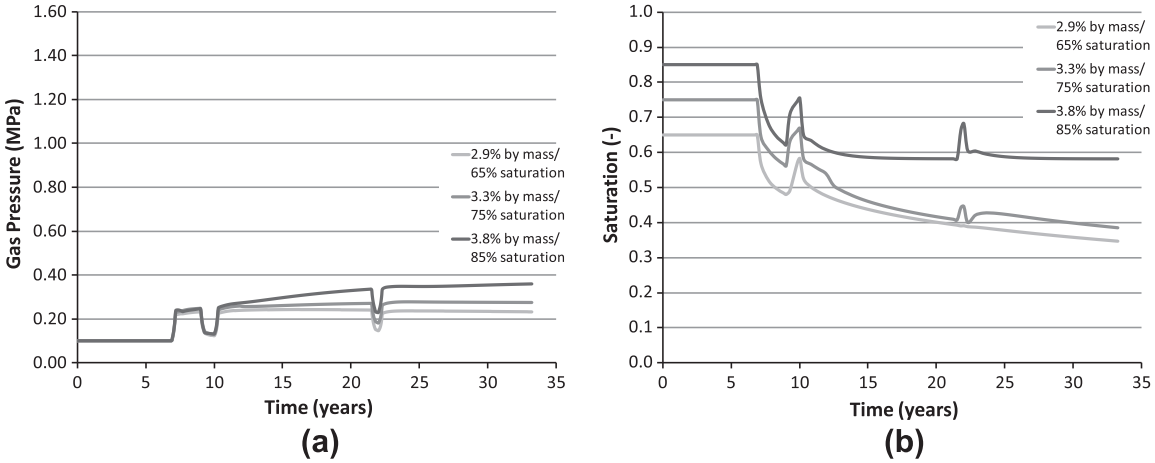

Fig. 9. Results of analyses with various moisture contents showing (a) gas pressures at the inner boundary in time and (b) the liquid water saturation at the inner boundary in time.

Concretes of similar porosity may have different permeabilities and laboratory testing is therefore the only realistic way of determining a value.

As with porosity, a very wide range of values for permeability are quoted in the literature ranging across six orders of magnitude from $10^{-16}\,m^2$ to $10^{-21}\,m^2$ for ordinary concretes and from $10^{-18}\,m^2$ to $10^{-22}\,m^2$ for high performance concretes (see Fig. 1). Again, there is little identifiable pattern to the quoted values other than, as would be expected for a denser material, HPC tends to have lower predicted values (but still ranging over four orders of magnitude). This again means that, from an analysis point of view, it is difficult to choose an appropriate value for a particular concrete.

Therefore, to determine the significance of the permeability for the behaviour of the PCPV three separate analyses were conducted with permeabilities of $1.0 \times 10^{-16}\,m^2$, $2.0 \times 10^{-18}\,m^2$ and $1.5 \times 10^{-21}\,m^2$.

From the results shown in Fig. 10a it can be seen that the permeability had a significant effect on the predicted gas pressures. As discussed previously, for the original permeability the gas pressures peaked at around 0.3 MPa after about 25 years before slowly decreasing. With the highest permeability, gas pressures reached little more than 0.15 MPa, peaking after each heat-up phase before dissipating quickly to an almost steady state condition. With the lowest permeability the gas pressures continued to rise over the life time of the structure, and as has been discussed before this is a persistently worsening situation. However, the peak pressure, reached after about 33 years, is around 1.05 MPa. This pressure is significant, not just because of the very large effect it shows the permeability to have of the gas pressure behaviour, but also because the magnitude of the pressure is of an order similar to the tensile strength of the concrete. If these conditions prevailed then, in contribution with other (mechanical) stresses, it is conceivable that damage could be incurred in the concrete near the steel liner. The load acting on the liner itself is also perhaps of concern.

In considering the moisture content (Fig. 10b) it can be seen that for the lowest permeability concrete, the drying process is very slow and very little moisture is lost even after 30+ years of operation. In fact it can be seen that the moisture content increased slightly upon first heat up. This is a result of a change in the equilibrium conditions within the concrete as vapour, formed from evaporating liquid water, is restricted from moving away from the heated part of the structure.

In contrast it may be seen that the highest permeability concrete dries relatively very quickly and appears to reach a steady state a few years after each outage. It may be interesting to note

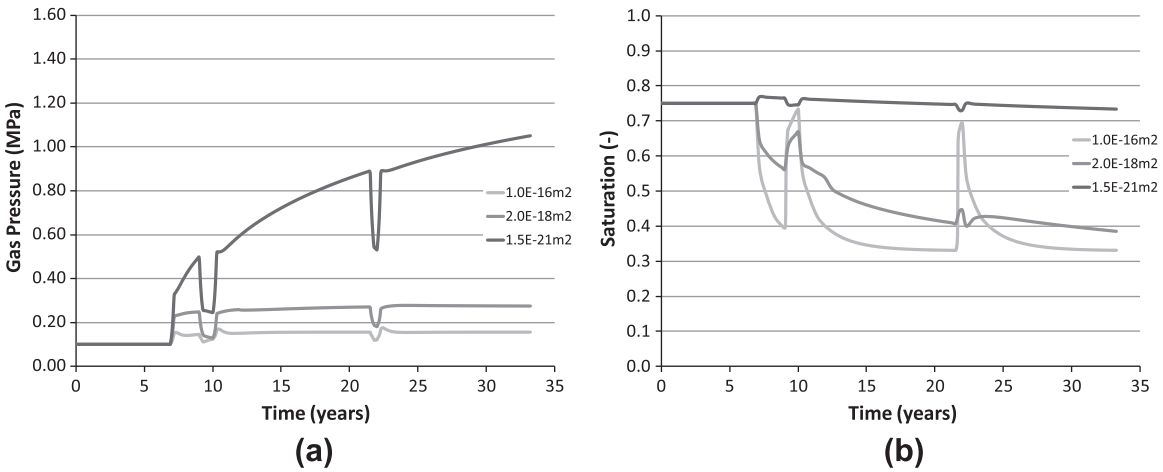

Fig. 10. Results of analyses with various permeabilities showing (a) gas pressures at the inner boundary in time and (b) the liquid water saturation at the inner boundary in time.

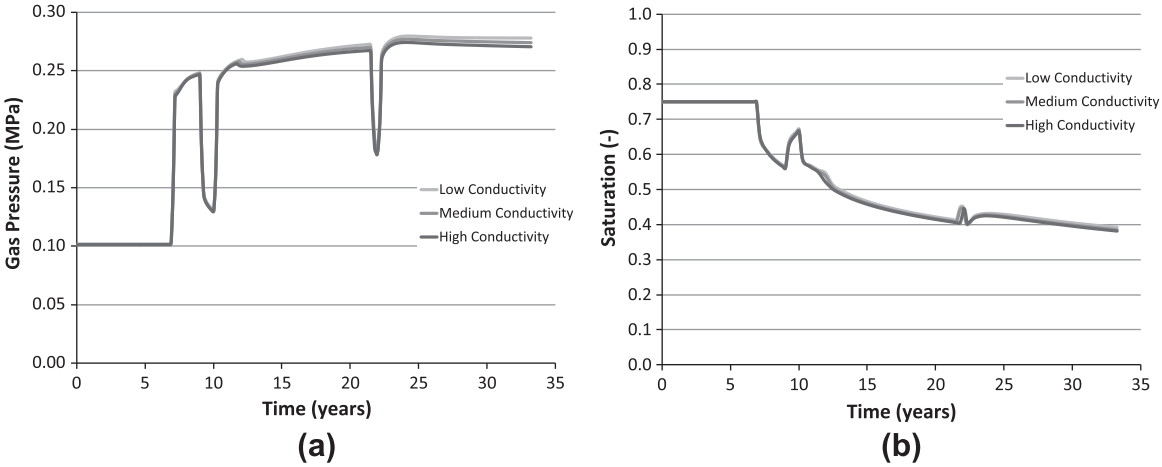

Fig. 11. Results of analyses with various thermal conductivities showing (a) gas pressures at the inner boundary in time and (b) the liquid water saturation at the inner boundary in time.

however that it also recovers moisture content much more quickly during cool downs than lower permeability concretes as vapour is able to move readily back into the cooling concrete.

4.2.4. Thermal conductivity

The thermal conductivity of the concrete is also a property about which little can be determined without experimental testing. Thermal conductivity controls the rate at which heat transfers through the concrete and so indirectly affects the fluid transport and the development of gas pressures. Upper and lower bound temperature dependent curves, considered to represent a range appropriate for all concretes (ordinary and high strength), are presented in the Eurocode [19]. Although no guidance is given as to specifically when to use what level of curve, it is suggested that high strength concretes may have higher thermal conductivities than ordinary concretes but the UK National Annex states that the lower bound curve should be employed.

To determine the significance of the thermal conductivity for the behaviour of the PCPV three separate analyses were conducted using the upper, mid-range and lower bound Eurocode curves.

As can be seen from Fig. 11a, over the life time of the PCPV, the gas pressures at the inside surface were very slightly higher with lower thermal conductivities. This is a result of the slower dissipation of the heat from the inside face through the wall of the structure and the consequent increase in conversion of liquid water to vapour. This in turn resulted in slightly higher relative humidity, leading to a change in the equilibrium conditions and ultimately a slightly higher saturation (Fig. 11b).

However, it may be noted that the effects were minimal for this set of conditions, which involves relatively low temperatures acting over relatively long time periods, whereby near steady state conditions are achieved. Hence, thermal conductivities within the ranges suggested by the Eurocode may be considered of very low significance in terms of the structural behaviour of the PCPV under normal operating conditions.

Close examination of the temperatures in the structure over time show that the near steady state temperature profiles across the thickness of the wall were also minimally affected by the thermal conductivity with the temperature on the outside of the structure varying by less than one Kelvin from those shown in Fig. 8a. The temperatures within the wall of the structure can be seen to increasingly lag those at the inside surface with lower thermal conductivities, as would be expected. But again, the overall effects were minimal and for all analyses near steady state conditions were reached in a relatively short timescale relative to the life time of the PCPV.

4.2.5. Worst case conditions

While some of the factors investigated above have been shown to have minimal significance for the overall heat and mass transport behaviour in the PCPV several have been shown to represent a worsening condition over the life time of the PCPV in relation to a continuous build up of gas pressure (stress) within the concrete of the structure. For the ranges of property values that have been determined to be reasonable, and potentially unknown, for a given PCPV or similar concrete structure, a 'worst case' combination may be imagined whereby all of the most adverse conditions are found to be present.

To determine the significance of this 'worst case' combination an analysis was run, following the results of the previous four sets of analyses, with a porosity of 12.2%,[2] liquid water saturation of 95% saturation, a permeability of 3.0×10^{-21} m^2 and a thermal conductivity according to the lower bound curve of the Eurocode.

As can be seen from the results shown in Fig. 12a, the 'worst case' combination resulted in gas pressures of approximately 1.35 MPa, which, as was expected, were the highest yet predicted. Again, this pressure, although alone not a concern for the development of damage, is significant enough to warrant further consideration being as it is, of an order of magnitude comparable with the tensile strength of the concrete and continuing to rise over the life time of the structure. There is reason for concern that these pressures could, in time, contribute to the development of damage in the concrete, in combination with other stresses, and that the steel liner could be affected.

It may also be noted that the moisture content of the concrete remained very high throughout its life time (Fig. 12b).

4.3. Simplified slice analysis – operating conditions

The following section is concerned with the sensitivity of the behaviour of the PCPV to changes in operating conditions. As can be seen from the typical profiles shown in Fig. 4, the PCPV experienced two planned outages during its life time and during these

[2] While the 'worst' porosity considered in Section 4.2.1. was 16% and the 'worst' permeability considered in Section 4.2.3 was 1.5e^{-21} m^2, it is not realistic to consider a concrete with extremes of both high porosity and low permeability. To give a more realistic 'worst case', values for a concrete presented by Baroghel-Bouny et al. [8] have been used.

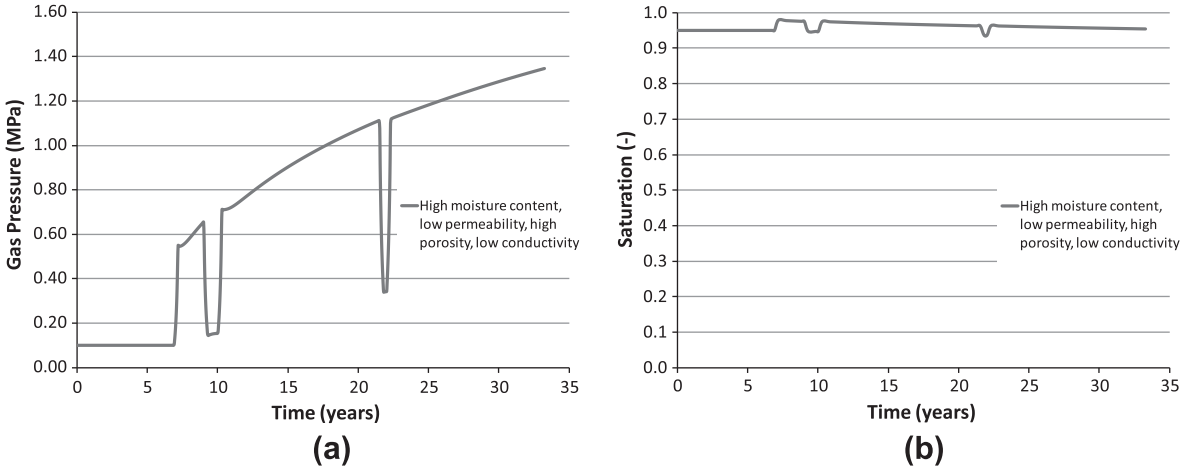

Fig. 12. Results of analyses with 'worst case' combination of porosity, moisture content, permeability and thermal conductivity showing (a) gas pressures at the inner boundary in time and (b) the liquid water saturation at the inner boundary in time.

periods the temperatures and internally applied pressure returned to normal, before increasing again upon reactor restart. Clearly these changes affect the heat and moisture transport in the structure of the PCPV and so, in order to identify implications for operational and management strategies, a series of analyses were conducted to determine the significance of various hypothetical changes to the operating conditions experienced by the structure during its life time. The factors investigated were the timings and length of the outages, the environmental conditions outside the structure and the extended operation of the PCPV. In each case results are presented (see Fig. 13a–n) using the typical properties and conditions, as employed above for the first analysis (Table 1), and using the 'worst case' conditions found in the previous section (Fig. 12a and b).

4.3.1. Timing of outages

Comparing the gas pressures predicted under the typical regime (Fig. 3) with earlier and later outages, and no outages at all, it can be seen in Fig. 13a that under typical conditions the predicted gas pressure, after the full life span of the PCPV, varied very little. After each outage the gas pressure peaked slightly before returning slowly to steady conditions. As a consequence of never peaking the predicted gas pressures with no outages were slightly lower than any of those with outages but the difference was minimal and given more time it is likely that all the predicted pressures would be the same.

In contrast, under 'worst case' conditions (Fig. 13c) the gas pressures predicted with no outages were higher than any of those with outages. This is because the occurrence of an outage, at whatever time, interrupts the otherwise continual rise in pressure predicted under 'worst case' conditions. Without outages the gas pressure effectively rises more quickly over the life time of the PCPV. Although still relatively small this difference could be significant if the pressures approached the tensile strength of the concrete. In that sense, although timing has little effect, any outages are beneficial to long term structural integrity.

Considering the moisture content, under typical conditions, drying occurs throughout the life time of the structure irrespective of the timing of the outages and does not reach steady state even after 30+ years (Fig. 13b). It is maximised where no outages occur to interrupt the process and minimised by later outages where recovery of moisture content occurs during cooling of the concrete. Under 'worst case' conditions (Fig. 13d), the outages have little effect and very little drying occurs over the life time of the structure.

4.3.2. Longer outages

The length of any particular outage will normally be governed by the reason for that outage; often planned maintenance. Fig. 13e shows the pressures predicted for extended outages under typical conditions and in comparison with the previous analyses it may be seen that the post outage peaks in pressure were higher. However, the pressure still returns to steady conditions given sufficient time and over the whole life time no difference was seen.

As above, the outages caused an interruption to the drying process and so longer outages resulted in a higher 'final' saturation (Fig. 13f), although, given time it is likely that drying would reach the same level as with shorter outages.

Fig. 13g shows the gas pressures predicted for extended outages under 'worst case' conditions. In this case the interruption in the gas pressure increase, discussed above, was extended and this had the effect of reducing the ultimate gas pressure even further. Thus longer outages, although not desirable from an economic, power generation point of view, may be better for the structure in the long term.

As before, longer outages had very little effect on the drying of the concrete with very little moisture lost over all (Fig. 13h).

4.3.3. Drier environment

The environmental conditions outside the PCPV clearly have an effect on heat and mass transfer out of the concrete. While typical conditions are reasonably well known and have been applied in most of the analyses in this work, it is feasible to control the atmospheric conditions surrounding the vessel and enforce a drier environment. (Other countries may of course have naturally drier environments.) Here the relative humidity outside the PCPV was reduced from 70% to 50%.

Intuitively, a drier environment will promote transport of vapour out of the concrete, increasing the rate of evaporation inside the concrete (drying) and result in lower gas pressures and lower saturation. As can be seen in Fig. 13i and j, under typical conditions this is the case. The relatively high permeability allowed the vapour to escape rapidly as it was driven towards the outside of the structure by an increased drying gradient (even before first heat up). This reduced the gas pressure at the steel liner significantly and therefore reduced the likelihood of damage.

However, as can be seen in Fig. 13k and l, under 'worst case' conditions the opposite is true. The increased drying gradient drove vapour more quickly towards the outside of the structure but the low permeability did not allow it to escape the structure as quickly as under typical conditions and almost no drying

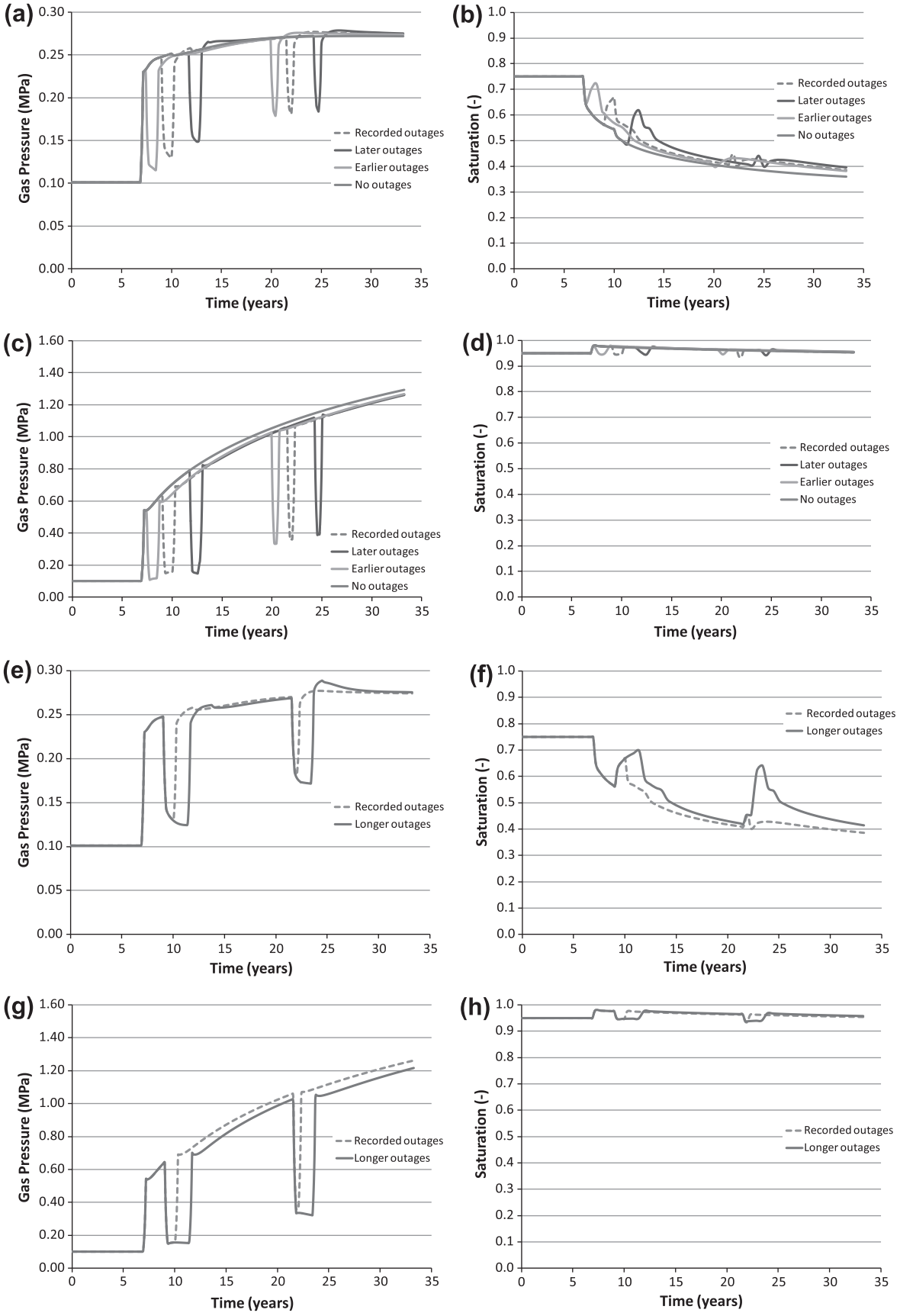

Fig. 13. Results showing gas pressures and the liquid water saturation at the inner boundary in time (a and b) with various outage timings under original conditions, (c and d) with various outage timings under 'worst case' conditions, (e and f) with longer outages under original conditions, (g and h) with longer outages under 'worst case' conditions, (i and j) with drier environmental conditions under original conditions, (k and l) with drier environmental conditions under 'worst case' conditions, (m and n) for extended operation under original and 'worst case' conditions.

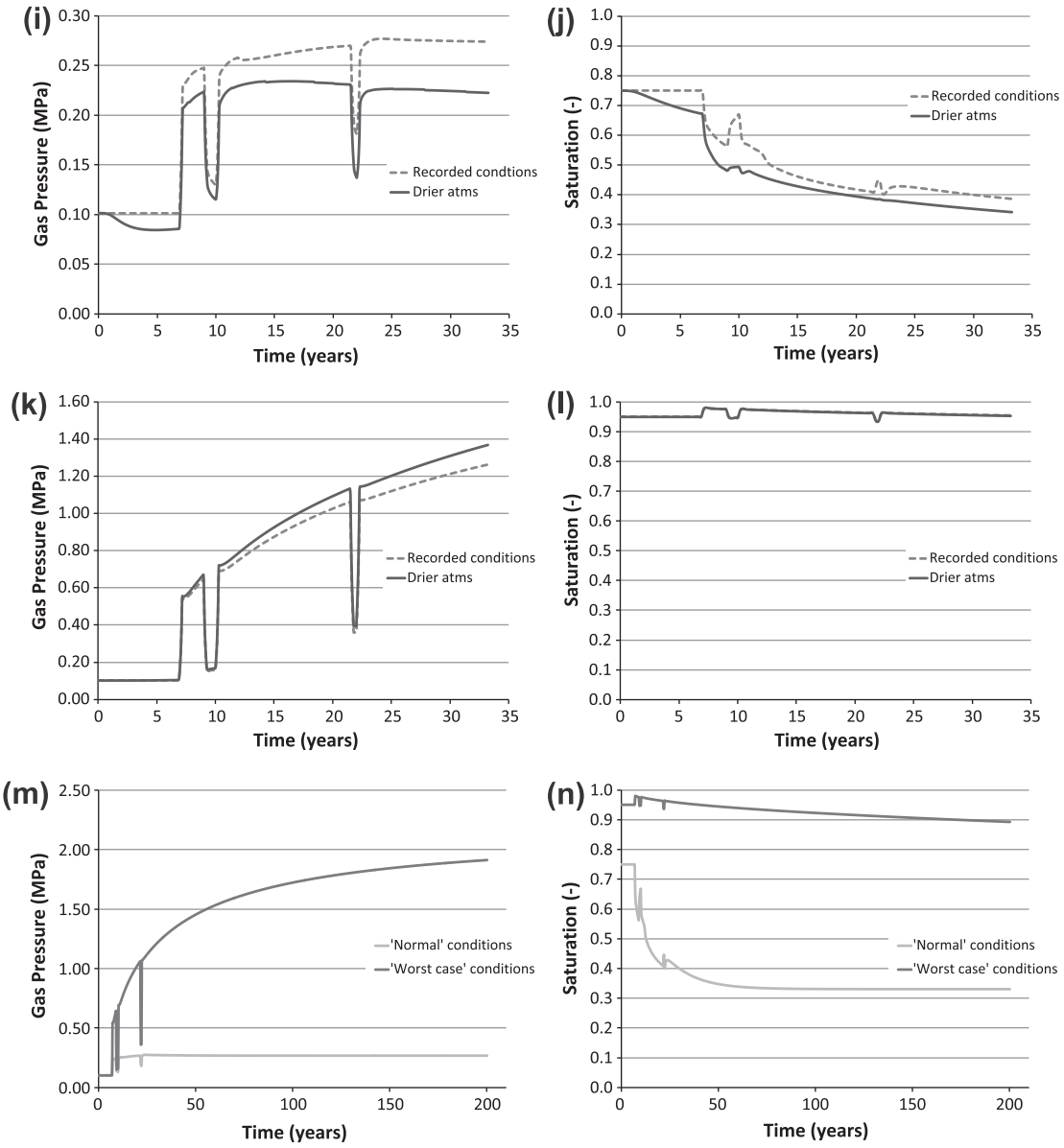

Fig. 13 (*continued*)

occurred. Instead the concrete fills with more vapour and the effect is to increase the saturation slightly and the gas pressure by a significant amount at the steel liner. Thus, attempting to dry the concrete of the PCPV by controlling the environmental conditions could theoretically induce damage in the structure.

4.3.4. Continued operation – life extension

One of the possible solutions to the requirement for increased energy demand in the UK and elsewhere is to extend the life of existing nuclear power plants. Given the findings of the analyses previously discussed in this work, two analyses were run to examine the behaviour of the PCPV if it were to continue operating. To illustrate the behaviour in the extreme an extended life time of 200 years was analysed. As can be seen in Fig. 13m and n, under typical conditions, the gas pressures reached equilibrium after less than 50 years of operation with the saturation following after around 70 years. Thereafter a constant relatively low level of pressure and saturation were maintained. However, under 'worst case' conditions it can be seen that, while drying was occurring at a slow rate, the gas pressure continued to rise. Although the trend was levelling it had not reached equilibrium even after 200 years and the pressure was approaching 2 MPa. This, in conjunction with the findings of the first analysis (Figs. 5–7), suggests that there may be limitations to the capacity for life extension of existing PCPVs and that before significant life extension can be considered detailed investigation and analysis should be carried out, taking into account the key material properties and operating conditions over the life time of the structure, in order to provide a rational assessment.

4.4. Temperature excursions

A further concern for operators is the possibility of temperature excursions, similar to those experienced at the Fukushima **Dai-ichi** power plant in Japan, whereby, due to a full or partial loss in cooling, the temperature in the PCPV can rise to temperatures perhaps in the region of 250 °C.

To examine the effects of such temperature excursions at different points during the life time of the PCPV in the context of the analyses previously presented and by way of demonstrating the capabilities, versatility and potential of the numerical tool employed here, nine separate analyses have been conducted. The first six, conducted using the simplified slice model, as before consider the gas pressures developed at the inside surface of the structure under typical and 'worst case' conditions. The second three, conducted using the full axi-symmetric model, consider the mechanical response and in particular the mechanical damage that develops under typical conditions. In each case it is assumed that the reactor is shut down following the incident and undergoes an outage before being restarted to normal operation.

4.4.1. Simplified slice analysis

As can be seen in Fig. 14 and as may be expected, during all six excursions, at early life, mid-life and late life, a significant spike developed in the gas pressure corresponding to the increase in temperature. Under typical conditions (Fig. 14a) these spikes exceeded 1.2 MPa in all cases and 1.4 MPa during the early-life excursion where more water remained in the concrete, but generally decrease with later life. Under 'worst case' conditions these spikes increased with later life and ultimately exceeded 3.0 MPa (Fig. 14c). As noted previously, pressures of these magnitudes are likely to result in damage to the concrete or steel liner.

It may be further noted that the behaviour of the structure changed following the excursions. In the case of typical conditions, rather than returning to the pre-excursion levels the gas pressures recovered to much lower levels. This is because the permeability of the concrete increased as a result of the thermal damage that the concrete suffered during the excursion; i.e. degradation of the material due to heating. Similar damage occurred under 'worst case' conditions but, because of the initially very low permeability, rather than dropping, the gas pressures continued to rise but at a decreased rate. It is also noticeable in this case that, during the outages following the temperature excursions, the gas pressures did not drop by much and in some cases rose. This is again a function of the low permeability. During the excursion a lot of vapour was produced by evaporation and this was not easily dissipated even when the structure cooled during outages. The pressure increase during outages was a result of the flow of vapour changing direction and flowing back towards the steel liner as the pressure gradients changed.

The spikes in gas pressure were accompanied by changes to the saturation (Fig. 14b and d). Under typical conditions there are significant drops in the moisture content as water is evaporated and expelled from the structure under high temperature gradients, aided by high permeabilities in the thermally damaged concrete. Under 'worst case' conditions the changes are less pronounced but increases in the drying rates can be observed due to the increased (although still relatively low) permeability of the post excursion, damaged concrete.

4.4.2. HTM analysis of PCPV

Examining the results of the full analyses (Fig. 15) it can be seen that, in all three cases, large zones of mechanical damage developed on the outside of the PCPV. As before these were a result of tensile stresses caused by the outward bending of the structure under the influence of internally applied pressures and restrained thermal expansion. The damaged areas were far more extensive

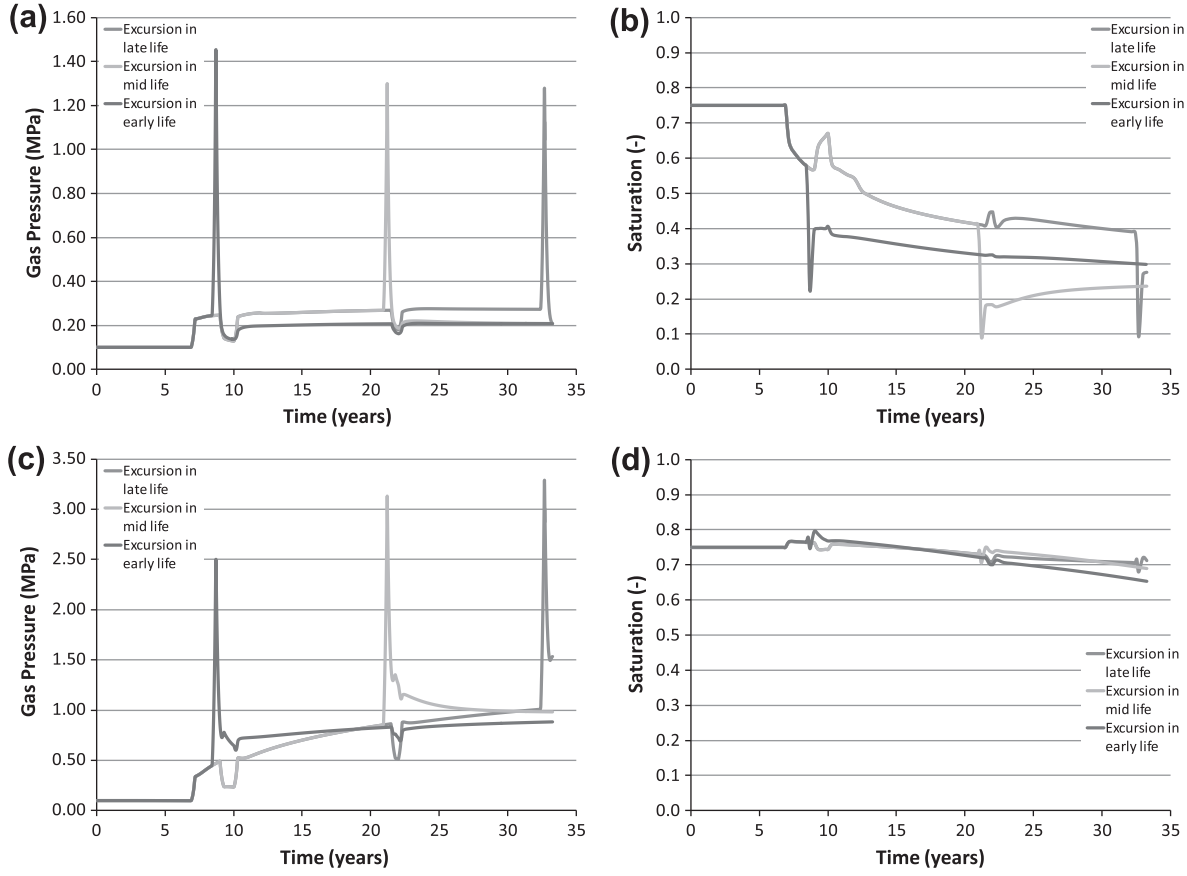

Fig. 14. Results of analyses of temperature excursions at early life, mid-life and late life showing gas pressures and the liquid water saturation at the inner boundary in time (a and b) with original conditions, (c and d) with 'worst case' conditions.

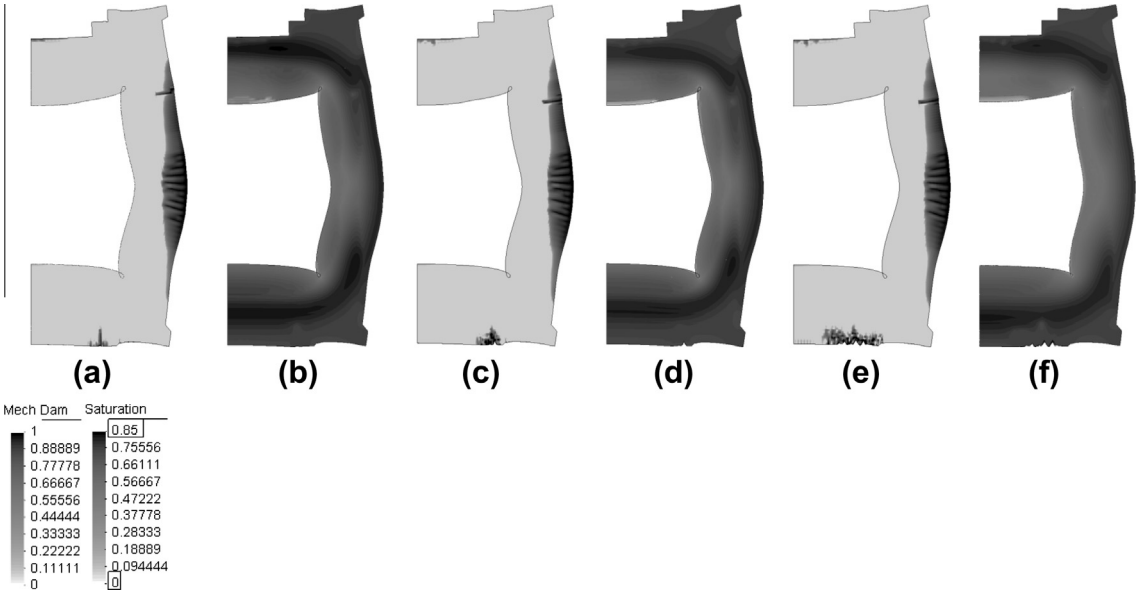

Fig. 15. Deformation of structure at an exaggerated scale (×450) showing mechanical damage and liquid water saturation resulting from temperature excursions at (a and b) early life, (c and d) mid-life, (e and f) late-life.

than those seen under original conditions (Fig. 4g), stretching over most of the height of the structure and up to 3 m into the wall. Other areas of the structures, around the top and base, were also seen to be damaged and it is notable that, while the large damage zone to the outside of the structure is similar after all three excursions, the zone of damage at the base is seen to increase in size as the excursions occur increasingly later in the life of the structure.

As a result of the significant softening of the damaged concrete the deformations of the structure were also greater. Whereas the maximum lateral deformation under typical conditions was around 1.3 mm, deformations under early-, mid- and late-life excursions were around 6.7, 7.2 and 7.4 mm respectively. As before, the increase in deformation with the later-life excursion can be attributed to creep in the pre-stressing tendons combined with the effects of transient thermal creep in the concrete.

The moisture content of the concrete is also affected by the temperature excursions although it is similarly influenced in all three stages of life. Rapid drying takes place near the hot interior of the structure and a ring of increased saturation develops from the middle outwards as vapour from the centre is driven out by high temperature gradients and subsequently re-condenses in the cooler parts of the concrete. This effect is reduced in the damaged areas where permeability in higher, allowing the vapour to dissipate.

These results, in combination with the thermal damage caused by the high temperatures to which the concrete were exposed, indicate a potentially significant threat to the structural integrity of the PCPVs and clearly again, further detailed analysis should be carried out in order to provide a rational assessment.

However, it must be emphasised that this is an extreme and simplified analysis, representative of a total and uniform loss of cooling. Other specific excursions may be more localised and less extreme but nonetheless these analyses again serve to illustrate the capabilities of the model in predicting the fully coupled, long-term, HTM behaviour of such structures.

5. Conclusions

This work has shown the modelling of the hygro-thermo-mechanical behaviour of a typical PCPV, generically similar to several currently in operation in the UK, over its full 30+ year life time. Through extensive parametric and sensitivity studies it has been shown that an understanding of the long-term behaviour of these safety–critical structures in response to variations in material properties and loading conditions is extremely important if current structures are to be considered for life extension and new build designs are to be optimised. The capabilities of the fully coupled, HTM model have been demonstrated and the following conclusions in relation to the current state of existing structures and the design and operation of new build structures may be drawn:

- Analysis of the typical structure over its full life time showed that some damage had gradually developed due to outwards bending of the walls under normal operating conditions. This was largely a result of the changes to the concrete and the diminishing pre-stress loads and was not considered to be significant in terms of the structural integrity or safety of the structure at present. However, the findings suggest that further detailed analysis is required in order to provide a rational assessment for life extension.
- The parametric study considering material properties that are typically less well characterised showed that under certain conditions gas pressures in the concrete (which may contribute adversely to the stress state in the structure, ultimately leading to the development of damage) may continue to increase over the whole life-time of the structure, representing a worsening case over the operating life time. It is feasible that these pressures may exceed 1 MPa.

Permeability, which may be the least well characterised property of the concrete, was found to have the largest and most significant effect on the gas pressures, while the porosity, moisture content and thermal conductivity were found have more limited and respectively decreasing effects. The ‘worst case’ conditions, potentially leading to gas pressures of over 1.3 MPa, were found to be concrete of low permeability, high porosity, high moisture content and low thermal conductivity. These factors and the control of these properties should be considered when designing new build structures.

- The sensitivity study found that only minor changes were seen in the development of gas pressures as a result of changes to the operating procedures. Outages of any length had minimal effect at low pressures but acted to interrupt and delay the development of persistently increasing gas pressures. In that sense, outages were found to be beneficial for the long term prevention of damage. Changes to the environmental conditions outside the PCPV had the potential to beneficially or adversely affect the behaviour depending on the properties of the concrete.
- Temperature excursions, as may occur as a result of a loss of cooling, were found to potentially have very significant effects for the PCPV. Under analyses representing very extreme cases it was found that very high gas pressures could develop within the concrete potentially damaging the structure and the steel liner. Extensive thermal and mechanical damage were found to occur in the concrete walls of the structure affecting its strength and stiffness and certainly requiring further detailed analysis in order to provide a rational assessment for continued operation.

Acknowledgements

This work was carried out with the aid of funding from the European Community through the MAECENAS research project "Modelling of ageing in concrete nuclear power plants" (FIKS-CT-2001-00186) and UK Engineering and Physical Sciences Research Council research project "An Advanced Numerical Tool for the Prediction and Analysis of Spalling in Concrete Structures Exposed to Combined Thermal and Mechanical Loading" (EP/E048935/1). The significant contribution of Mr Adam Gibson is also gratefully acknowledged.

Appendix A

Full details of the parametric relationships employed in the model can be found in [6,7,17]. Brief details for some key parameters are given here.

Intrinsic permeability:

$$K = K^0(10^{4D}) \tag{AI.1}$$

where K^0 is the initial permeability, and $D = \omega + \chi - \omega\chi$ is the multiplicative thermal (χ)-mechanical (ω) damage.

Thermal conductivity [19]:

$$k = k_1 - k_2\left(\frac{T_C}{100}\right) - k_3\left(\frac{T_C}{100}\right)^2 \tag{AI.2}$$

where the coefficients $k_1 = 1.68$, $k_2 = 0.19055$ and $k_3 = 0.0082$.

Moisture content – Sorption Isotherms (8) (adapted from [21]):

$$\varepsilon_L = \begin{cases} \left(\frac{\varepsilon_{Cem}\rho_{Cem}}{\rho_L}\right)\left(\frac{\varphi^0\rho_L^0}{\varepsilon_{Cem}\rho_{Cem}}\frac{P_V}{P_{Sat}}\right)^{1/m} & \text{for } \left(\frac{P_V}{P_{Sat}}\right) \leqslant 0.96 \\ a\left(\frac{P_V}{P_{Sat}}\right)^3 + b\left(\frac{P_V}{P_{Sat}}\right)^2 + c\left(\frac{P_V}{P_{Sat}}\right) + d & \text{for } 0.96 < \left(\frac{P_V}{P_{Sat}}\right) < 1.00 \\ \varphi & \text{for } \left(\frac{P_V}{P_{Sat}}\right) = 1.00 \end{cases} \tag{AI.3}$$

where ϕ^0 is the initial porosity of the concrete, rho_L^0 is the initial density of liquid water, a, b, c and d are complex temperature dependent coefficients of a cubic function such that ε_L and its derivatives are always continuous, and m is a temperature dependent coefficient given by (AI.4):

$$m = 1.04 - \frac{(T_C + 10)^2}{(T_C + 10)^2 + 22.3(25 + 10)^2} \tag{AI.4}$$

where T_C is the temperature in degrees Celsius.

Coefficient of Load Induced Thermal Strain (13):

$$\beta = 0.01 \times \begin{cases} 2X\theta + Y & \text{for } 0 \leqslant \theta \leqslant \overline{\theta} \\ 2Z(\theta - \overline{\theta}) + 2X\overline{\theta} + Y & \text{for } \theta > \overline{\theta} \end{cases} \tag{AI.5}$$

where X, Y and Z are coefficients of a bi-parabolic function.

Tensile strength:

$$f_t = f_t^0(1 - 0.1\widehat{\theta})^2 \tag{AI.6}$$

where f_t^0 is the initial tensile strength of the concrete and $\widehat{\theta} = \max(\theta)$, where θ is a normalised temperature defined by:

$$\theta = \frac{T - T_0}{100} \tag{AI.7}$$

References

[1] Committee on Climate Change. The renewable energy review; 2011, London, UK. <http://www.theccc.org.uk/reports> [accessed 28.08.12].
[2] Parliamentary Office of Science and Technology. Carbon footprint of electricity generation. PostNote, Update; 2011.
[3] United Nations. Kyoto Protocol to the United Nations Framework Convention on, Climate Change, Kyoto; 1998.
[4] Great Britain, Climate Change Act 2008, London, UK: The Stationery Office.
[5] IAEA. Mission Report: The Great East Japan Earthquake Expert Mission – IAEA International Fact Finding Expert Mission of the Fukushima Dai-Ichi NPP Accident Following the Great East Japan Earthquake and Tsunami. IAEA, Division of Nuclear Installation Safety, Department of Nuclear Safety and Security: Tokyo; 2011.
[6] Davie CT, Pearce CJ, Bicanic N. A fully generalised, coupled, multi-phase, hygro-thermo-mechanical model for concrete. Mater Struct 2010;43(Suppl. 1).
[7] Davie CT, Pearce CJ, Bicanic N. Coupled heat and moisture transport in concrete at elevated temperatures – effects of capillary pressure and adsorbed water. Numer Heat Transfer, Part A 2006;49(8):733–63.
[8] Baroghel-Bouny V et al. Characterization and identification of equilibrium and transfer moisture properties for ordinary and high-performance cementitious materials. Cem Concr Res 1999;29:1225–38.
[9] Tenchev R, Purnell P. An application of a damage constitutive model to concrete at high temperature and prediction of spalling. Int J Solids Struct 2005;42(26):6550–65.
[10] Schrefler BA et al. Concrete at high temperature with application to tunnel fire. Comput Mech 2002;29:43–51.
[11] Zeiml M et al. Thermo-hydro-chemical couplings considered in safety assessment of shallow tunnels subjected to fire load. Fire Saf J 2008;43(2):83–95.
[12] Ichikawa Y, England GL. Prediction of moisture migration and pore pressure build-up in concrete at high temperatures. Nucl Eng Des 2004;228(1–3):245–59.
[13] Gawin D, Pesavento F, Schrefler BA. Hygro-thermo-chemo-mechanical modelling of concrete at early ages and beyond. Part I: Hydration and hygro-thermal phenomena. Int J Numer Meth Eng 2006;67(3):299–331.
[14] Gawin D, Pesavento F, Schrefler BA. Hygro-thermo-chemo-mechanical modelling of concrete at early ages and beyond. Part II: Shrinkage and creep of concrete. Int J Numer Meth Eng 2006;67(3):332–63.
[15] Gawin D, Pesavento F, Schrefler BA. Simulation of damage-permeability coupling in hygro-thermo-mechanical analysis of concrete at high temperature. Commun Numer Methods Eng 2002;18:113–9.
[16] Gawin D, Pesavento F, Schrefler BA. Modelling of deformations of high strength concrete at elevated temperatures. Mater Struct 2004;37:218–36.
[17] Davie CT, Zhang HL, Gibson A. Investigation of a continuum damage model as an indicator for the prediction of spalling in fire exposed concrete. Comput Struct 2012;94–95:54–69.
[18] Crouch R. Modelling of Ageing in Concrete Nuclear Power Plant Structures (MAECENAS) project, final report. Department of Civil & Structural Engineering, University of Sheffield; 2005.
[19] CEN. BS EN 1992–1-2:2004 Eurocode 2: Design of concrete structures – Part 1–2: General rules – Structural fire design. European Standards. London; 2004.
[20] Pearce CJ, Nielsen CV, Bicanic N. Gradient enhanced thermo-mechanical damage model for concrete at high temperatures including transient thermal creep. Int J Numer Anal Meth Geomech 2004;28(7–8):715–35.
[21] Tenchev RT, Li LY, Purkiss JA. Finite element analysis of coupled heat and moisture transfer in concrete subjected to fire. Numer Heat Transfer – A 2001;39:685–710.